

# Multiwavelength monitoring and reverberation mapping of NGC 2617 at deepest minimum with a sharp upward turn during 2021–2024

V. L. Oknyansky<sup>1,2★</sup>, M. S. Brotherton<sup>3</sup>, S. S. Tsygankov<sup>4</sup>, A. V. Dodin<sup>1</sup>, A. M. Tatarnikov<sup>1,5</sup>, P. Du<sup>6</sup>, M. A. Burlak<sup>1</sup>, N. P. Ikonnikova<sup>1</sup>, V. G. Metlov<sup>1</sup>, A. A. Belinski<sup>1</sup>, N. I. Shatsky<sup>1</sup>, J. -M. Wang<sup>6,7,8</sup>, D. -W. Bao<sup>8</sup>, F. Fang<sup>6</sup>, S. Zhai<sup>6</sup>, Y.-X. Fu<sup>6,7</sup>, H.-R. Bai<sup>6,7</sup>, T. E. Zastrocky<sup>3</sup>, D. Chelouche<sup>2,9</sup>, C. Sobrino Figaredo<sup>2,9</sup>, S. Kaspi<sup>10</sup> and C. M. Gaskell<sup>11</sup>

<sup>1</sup>*Sternberg Astronomical Institute, M.V. Lomonosov Moscow State University, Universitetsky pr-t, 13, 119234 Moscow, Russia*

<sup>2</sup>*Department of Physics, Faculty of Natural Sciences, University of Haifa, Haifa 3498838, Israel*

<sup>3</sup>*Department of Physics and Astronomy, University of Wyoming, Laramie, WY 82071, USA*

<sup>4</sup>*Department of Physics and Astronomy, University of Turku, FI-20014 Turku, Finland*

<sup>5</sup>*Faculty of Physics, Moscow M.V. Lomonosov State University, Leninskie gory 1, Moscow 119991, Russia*

<sup>6</sup>*Key Laboratory for Particle Astrophysics, Institute of High Energy Physics, Chinese Academy of Sciences, 19B Yuquan Road, Beijing 100049, China*

<sup>7</sup>*School of Astronomy and Space Science, University of Chinese Academy of Sciences, 19A Yuquan Road, Beijing 100049, China*

<sup>8</sup>*National Astronomical Observatories of China, Chinese Academy of Sciences, A20 Datun Road, Beijing 100012, China*

<sup>9</sup>*Haifa Research Center for Theoretical Physics and Astrophysics, University of Haifa, Haifa 3498838, Israel*

<sup>10</sup>*School of Physics and Astronomy and Wise observatory, Tel Aviv University, Tel Aviv 6997801, Israel*

<sup>11</sup>*Department of Astronomy and Astrophysics, University of California, Santa Cruz, CA 95064, USA*

Accepted 2024 December 6. Received 2024 December 6; in original form 2024 August 1

## ABSTRACT

We present the results of a new X-ray to near-IR photometric and spectroscopic monitoring of the changing look active galactic nucleus NGC 2617 carried out from March 2022 to March 2024. We found significant variability at all wavelengths and in the intensities and profiles of the broad Balmer lines. Reverberation mapping was carried out for three observing seasons during 2021–2024. We obtained time delays of  $\sim 4$  d for the response of the  $H\beta$  line to optical continuum variations. The X-ray variations correlate well with the UV and optical, with a few days lag for longer wavelengths. The  $K$  band lagged the  $B$  band by  $\sim 15$  d during the last three seasons, which is significantly shorter than the delays reported previously by the 2016 and 2017–2019 campaigns. Near-IR variability arises from two different emission regions: the outer part of the accretion disc and a more distant dust component. The  $HK$ -band variability is governed primarily by dust. The  $H\beta/H\alpha$  ratio variations (for broad components only) correlate with the X-ray and UV fluxes. The spectral type changed from type 1.8 to type 1.9 during 2023 October–2024 January and then a more rapid change to type 1.5 occurred in 2024 February. We interpret these changes as a combination of two factors: changes in the accretion rate as a dominant cause but also the sublimation or recovery of dust along the line of sight.

**Key words:** galaxies: active – galaxies: individual: NGC 2617 – galaxies: Seyfert – optical: galaxies – X-rays: galaxies – UV.

## 1 INTRODUCTION

Active galactic nuclei (AGNs) can be classified into two broad categories (Antonucci 2012): ‘thermal’ AGNs with high Eddington ratios where the energy output is dominated by thermal emission from an accretion disc, and ‘non-thermal’ AGNs with much lower Eddington ratios where the energy output is dominated by mechanical energy in jets. Khachikyan & Weedman (1971) classified thermal AGNs on the basis of their optical spectra into type-1 AGNs, where both broad and narrow permitted lines are seen, and type-2 AGNs where only narrow lines are seen. This classification was refined by Osterbrock (1981) to add subclasses with properties intermediate

between type 1 and type 2: type 1.5 (Sy1.5) – objects which have clearly composite profiles of  $H\alpha$  lines with strong narrow and broad components; type 1.8 (Sy1.8) – objects with an easily visible broad  $H\alpha$  component, but only a very weak broad  $H\beta$  component; type 1.9 (Sy1.9) – objects with an easily visible broad  $H\alpha$  component, but with broad  $H\beta$  not visible at all. At present, there are no generally accepted numerical parameters for dividing objects into these intermediate classes.

Keel (1980) made the important discovery that type-1 and type-2 AGNs differ in orientation. From this, he deduced that there was an obscuring disc close to the AGNs such that the innermost parts of an AGN could be obscured but not the surrounding stars and extended emission. Keel pointed out that an obscuring ring with a polar half-opening angle of 60 deg and seen at various inclinations could explain the orientation difference he found between

\* E-mail: [victoroknyansky@gmail.com](mailto:victoroknyansky@gmail.com)

**Table 1.** The WIRO and CMO  $H\beta$  fluxes (in units of  $10^{-13}$  erg  $s^{-1}$   $cm^{-2}$ ). (Note: This table is available in its entirety in machine-readable form.)

J.D.-2450000	Flux in $H\beta$	Observatory
9640.81	$0.915 \pm 0.046$	WIRO
9641.74	$0.974 \pm 0.049$	WIRO
9642.76	$0.932 \pm 0.047$	WIRO
9649.68	$1.014 \pm 0.051$	WIRO
9654.62	$1.094 \pm 0.055$	WIRO
...	...	...

type-1 and type-2 AGNs. Keel’s discovery led to the now standard accepted orientation-dependent unification model of thermal AGNs (see Antonucci 1993 for a review). In this picture, all thermal AGNs are essentially the same but we do not see the accretion disc (AD) and broad-line region (BLR) directly if we are viewing from far off axis. An AGN appears to be a type 1 when viewed close to the axis of symmetry and a type 2 when viewed far off axis.

Although the orientation unification picture has long been accepted, spectral variability presents a major challenge. In the basic picture, such as the ‘straw-person model’ of Antonucci (1993), variation of the spectral class was not expected due to the long dynamical time-scales involved. However, Lyutyj, Oknyanskij & Chuvaev (1984) discovered that NGC 4151, which normally has

an optical spectral appearance of a type-1 AGN, looked like a type-2 AGN when at minimum light. Such a change is called a ‘changing look’ (CL). The CL phenomenon is now recognized to be very common and many examples can be found in the literature. In recent years, the number of observed CL events has exceeded 100, and CL events have started to be considered a not-too-rare phenomenon. The CL AGNs give us a view of extreme changes in the AGN state spanning a few weeks to years, which may provide insight into the major open questions about the nature of possible sources of fuel and AGN evolution.

A number of CL AGNs have a long history of investigations that reveals *recurrent* extreme variability of such objects. Examples include NGC 1566 (Pastoriza & Gerola 1970; Oknyansky et al. 2019a, 2021), NGC 3516 (Andrillat & Souffrin 1968; Shapovalova et al. 2019; Oknyansky, Mikailov & Huseynov 2020a; Oknyansky et al. 2021), NGC 4151 (Lyutyj et al. 1984; Penston & Perez 1984; Chuvaev & Oknyanskii 1989), Mrk 6 (Khachikian & Weedman 1971; Pronik & Chuvaev 1972; Chuvaev 1991), Mrk 590 (Denney et al. 2014; Raimundo et al. 2019; Lawther et al. 2022), and other sources. The investigation of such recurrent CL events is the main goal of the CL monitoring project (Oknyanskij et al. 2016) of which the present study is part. The common properties of the CL AGNs have been discussed by Shappee et al. (2014), Oknyansky (2022), Ricci & Trakhtenbrot (2023), and some others.

The CL phenomenon is clearly high-amplitude AGN variability, but there is little that is understood about AGN variability. Hence, little is understood about the physical nature of the CL AGN

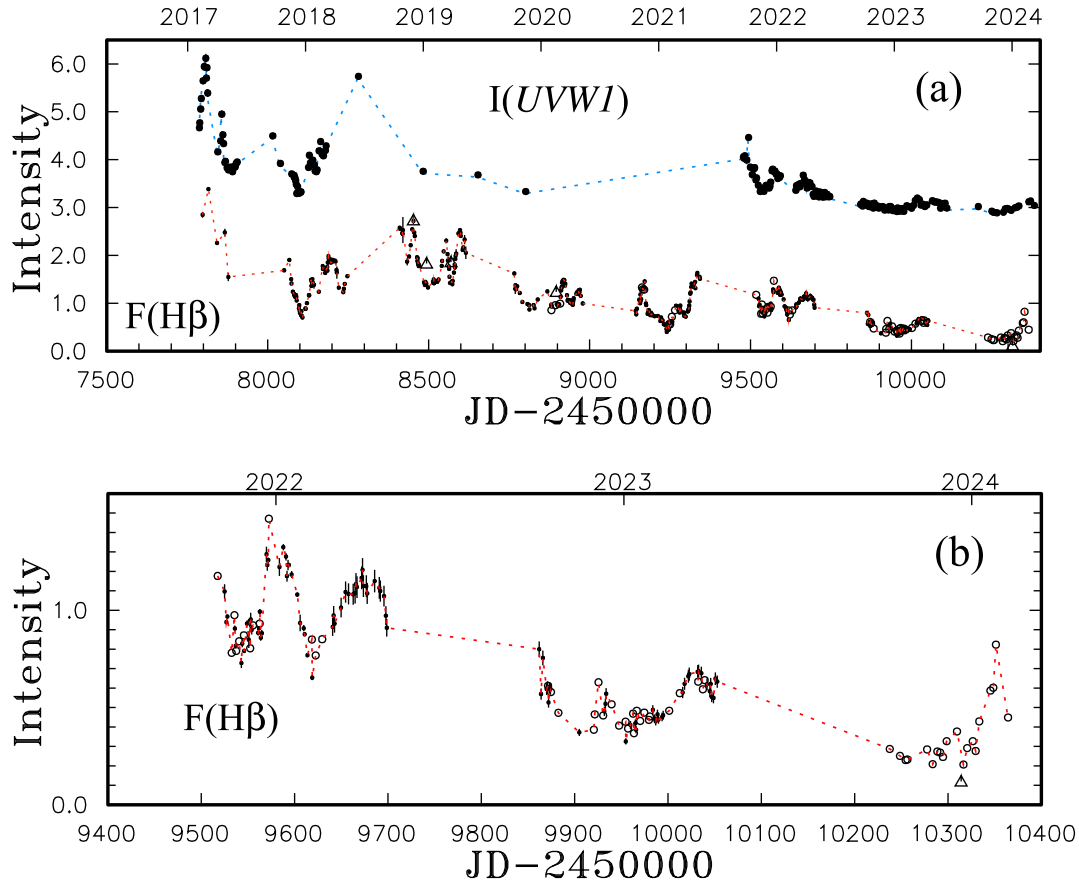


**Figure 1.** Variation of the  $H\beta$  flux in units of  $10^{-13}$  erg  $s^{-1}$   $cm^{-2}$  in 2017–2024 (a) and in 2021–2024 (b) (points correspond to the WIRO data, open circles –CMO, triangles–SAAO). The (a) panel also demonstrates the variation of the relative intensity in the  $UVW1$  (filled circles).

**Table 2.** The  $B$  photometry obtained with the 0.6-m telescope (DAS), the RC600 telescope (CMO), the 0.7-m telescope of the Wise observatory (Wis), and the *Swift* $B$  photometry (Swi). All data are reduced to the *Swift* $B$  system. (Note: This table is available in its entirety in machine-readable form.)

J.D.-2450000	Mag	
9640.900	$15.593 \pm 0.046$	Swi
9641.340	$15.501 \pm 0.018$	CMO
9642.820	$15.475 \pm 0.034$	Swi
9643.280	$15.476 \pm 0.018$	CMO
9645.298	$15.513 \pm 0.019$	CMO
...	...	...

phenomenon. When the first CL events in AGNs were discovered (Khachikian & Weedman 1971; Pronik & Chuvayev 1972; Lyutyj et al. 1984), two possible mechanisms were suspected to be responsible for these dramatic changes of the spectral type: (1) accretion-rate variability and (2) variable obscuration. The latter possibility is disfavoured for some cases based on the time-scale of the transition (see e.g. LaMassa et al. 2015; MacLeod et al. 2016), but it could be responsible for other cases of CL behaviour. The two mechanisms could also act together, if we take into account the possibility of fast (occurring on a time-scale much shorter than the dynamical time-scale) sublimation or (and) recovery of dust in some clouds along the line of sight, which follows (with some delay) the strong UV-flux variations (as the primary reason; see e.g. Oknyansky, Gaskell & Shimanovskaya 2015; Oknyansky et al. 2017a; Oknyansky, Malanchev & Gaskell 2018; Kokubo & Minezaki 2020; Oknyansky & Gaskell 2024). It is possible that there are two different subclasses of CL AGNs (Ricci & Trakhtenbrot 2023).

Gaskell & Klimek (2003) raise the question of whether AGNs have what they call variability ‘personalities’ (i.e. intrinsically different variability properties) or whether we are just seeing ‘moods’ (e.g. there are only some time intervals when there is greater or lesser variability). The same question applies to so-called CL AGNs. Thus, it is not clear if the objects with observed CL events form a separate subclass of variable AGNs or are similar objects but caught at the most extreme moments of their variability (see discussion and references in Runnoe et al. 2016; Oknyansky et al. 2017a, 2019a, 2021, 2023a; MacLeod et al. 2019; Ruan et al. 2019; Wang & Bon 2020; López-Navas et al. 2023; Veronese et al. 2024). Klimek, Gaskell & Hedrick (2004) found that narrow-line Seyfert 1s (NLS1s), which have very high Eddington ratios, are less variable than lower Eddington ratio AGNs. Similarly, CL AGNs have low Eddington ratios (usually a few per cent or less). They also tend to be relatively X-ray brighter than the overall type-1 population.

To investigate these questions, we have been carrying out long-term, multiwavelength monitoring of NGC 2617 (Oknyansky et al. 2017a, 2023a, hereinafter Papers I and II, respectively). Intensive multiwavelength observations of NGC 2617 were triggered by the discovery (Shappee et al. 2014) of a CL event in 2013 (Mathur et al. 2013; Tsygankov et al. 2013; Yang et al. 2013; Shappee et al. 2013b; Fausnaugh 2017; Giustini et al. 2017; Sheng et al. 2017; Oknyansky et al. 2017a, b; Fausnaugh et al. 2018; Olson et al. 2020; Feng et al. 2021; Yang et al. 2021). From the first mention of NGC 2617 by Edouard Jean-Marie Stephan back in 1885 until 2013, it was observed very rarely and only two optical spectra were published (Moran, Halpern & Helfand 1996; Paturel et al. 2003). These two spectra gave a classification of type 1.8 (see Osterbrock 1987). Subsequent spectroscopic observations allowed Shappee et al. (2014) to detect a large change of spectral type (i.e. a CL event) over

the period 2003 to 2013, from type 1.8 in the old spectra to type 1. We proposed (using the MASTER photometry; Oknyansky et al. 2017a) that the type change had probably occurred between 2010 October and 2012 February, which was also independently suspected by Sheng et al. (2017) using mid-IR photometry.

We began spectroscopic and photometric (IR  $JHK$ , optical  $BVR$ ) monitoring of NGC 2617 in 2016 January to trace potential recurrent state changes (see details and references in Paper I) and published our results of long-term monitoring in Paper II. The present work is a continuation of Papers I and II; it is based mostly on unpublished data and focuses on the variability of NGC 2617 during the last three observing seasons (2021–2024), when the object returned to a very low state which can be classified as type 1.9, and the X-ray flux reached the lowest value ever observed (Oknyansky et al. 2023b). Such an event was expected since 2013 after the significant brightening and CL event was discovered by Shappee et al. (2014). We also compare the recent deep minimum with the previous one that occurred at the end of 2017.

We here present our new observational data on the X-ray/UV/optical/IR continuum and optical emission-line variability of NGC 2617 obtained by the *Swift* satellite, at the Caucasian Mountain Observatory (CMO) of SAI MSU, the Wyoming Infrared Observatory (WIRO), the Dibai E.A. Astronomical Station (DAS) of SAI MSU, and at the Wise Observatory from March 2022 till 2024 February. We also perform reverberation mapping (RM) of the 2021–2024 data to investigate time lags between variable emission components at different wavelengths, including those associated with the  $H\beta$  broad emission line.

## 2 OBSERVATIONS, INSTRUMENTS, AND DATA REDUCTION

In Papers I and II, we reported the results of spectroscopic and photometric monitoring over the period 2016 January–2022 February. In the present study, we combine our old data with new data obtained partly with the same telescopes, but with some differences and additions.

### 2.1 Spectroscopy

The 2.3-m telescope at WIRO provided 281 epochs of spectroscopy in 2016–2022 (published in Paper II) and 58 new epochs in 2022–2023. Our methods and procedures are the same as previously reported (see Du et al. 2018). Additionally, the 2.5-m telescope at CMO provided 23 epochs of spectroscopy during 2020–2022 (published in Paper II) and 43 new epochs in 2022–2024. The instrumentation and methods are as previously reported (see Oknyansky et al. 2021, 2023a). Finally, the 1.9-m telescope at SAAO (South Africa) provided four epochs of spectra in 2017–2018 and one additional spectrum in 2024. Oknyansky et al. (2019b) provides more detailed information about the data from this facility.

Due to different apertures at the different observatories, we have made some corrections for consistency. In particular, we used a linear regression to reduce the  $H\beta$  fluxes to be consistent with the WIRO system. Table 1 gives the new data, and Fig. 1 presents the  $H\beta$  flux light curve during the last three seasons (2021–2024) along with the combined  $H\beta$  light curve for 2017–2024.

### 2.2 *Swift* X-ray, UV, and optical data

Papers I and II present 120 epochs of *Swift* data obtained between June 2016 and January 2022, which included both X-ray fluxes and

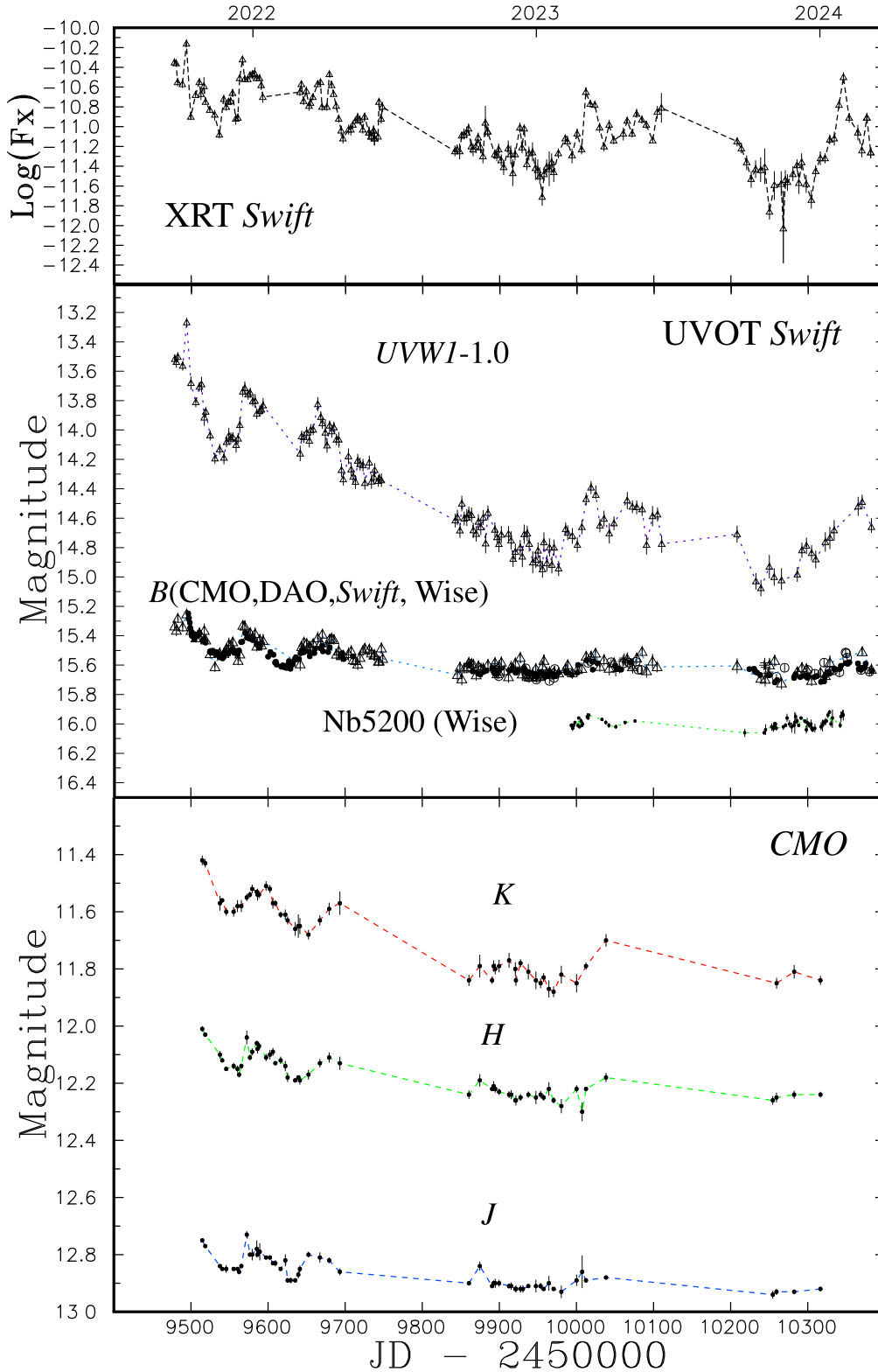


**Figure 2.** Multiwavelength observations of NGC 2617 in 2021–2024. Top panel: The *Swift*/XRT 0.5–10 keV X-ray flux (in units of  $\text{erg cm}^{-2} \text{s}^{-1}$ ). Middle panel: The *Swift* data for a 10-arcsec aperture (diameter) are shown with triangles connected by a dashed line for the UVW1 data and a dashed line for the B data. Besides the *Swift* data (triangles), the B data obtained at different observatories are also shown: DAS (open circles), CMO (nightly mean estimates), and Wise (crosses). All the B magnitudes were measured in an aperture of 10 arcsec and reduced to the *Swift*B system. The narrow-band NB5200 photometry obtained at Wise (the data are given in magnitude scale with arbitrarily selected zero-point) is shown with points connected by a dashed line. Bottom panel: The near-IR light curves in J, H and K obtained at CMO (for an aperture (diameter) of 5 arcsec).

**Table 3.** The NB5200 photometry with 10-arcsec aperture obtained with the 0.8-m telescope of the Wise observatory. The data given on a magnitude scale with an arbitrarily selected zero-point as presented at Fig. 2. (Note: This table is available in its entirety in machine-readable form.)

J.D.-2450000	Mag
9992.475	16.013 ± 0.012
9993.271	16.009 ± 0.015
9994.280	16.025 ± 0.023
9995.444	16.010 ± 0.013
9997.283	15.994 ± 0.009
...	...

UV/optical photometry. We give here more recent *Swift* observations from March 2022 to March 2024: X-ray (XRT, 131 epochs), *UVW1* (UVOT, 110 epochs), and *B* (UVOT, 106 epochs). The methods were the same as in Papers I and II, but we used updated calibrations and software and the older data were reprocessed for uniformity. It should be noted that the *Swift* UVOT data obtained through the last two seasons often had problems due to poor stabilization of the observatory. Therefore, we visually inspected the quality of the images and did not use photometry with low-quality data. All optical and UV *Swift* photometry corresponds to a 10 arcsec aperture (hereinafter, the diameter of the aperture is meant).

### 2.3 Ground-based optical photometry

We present new optical photometry in Table 2 and Fig. 2. Observations were obtained with the 0.6-m telescope at CMO (124 epochs) and the 0.6-m telescope at DAS of SAI MSU (37 epochs) over the period March 2022–February 2024. Details about the methods and instruments can be found in Paper II. Additionally,

**Table 4.** *JHK* photometry obtained with the 2.5-m telescope (CMO). (Note: This table is available in its entirety in machine-readable form.)

J.D.-2450000	Mag	Band
9679.219	12.110 ± 0.018	<i>H</i>
9679.219	12.820 ± 0.010	<i>J</i>
9679.227	11.590 ± 0.022	<i>K</i>
9693.191	12.860 ± 0.012	<i>J</i>
9693.195	11.570 ± 0.041	<i>K</i>
...	...	...

we present 12 epochs of new *B*-band photometry obtained at the Wise Observatory with the 0.7-m Centurion 28 (C28IL) telescope (see details in Brosch et al. 2015) and 69 epochs of narrow-band NB5200 observations made with the newly-commissioned 0.8-m H80 telescope (see filter definition in Pozo Nuñez et al. 2017). The narrow-band NB5200 photometry on a magnitude scale with an arbitrarily (for clarity) selected zero-point is given in Table 3 and Fig. 2. All optical photometry corresponds to a 10-arcsec aperture. All *B*-band photometric data were reduced to the *Swift* *B* system (see Table 1).

### 2.4 Near-IR photometry

Papers I and II reported 194 epochs of near-IR *JHK* data obtained in 2016–2022 with the ASTRONIRCAM camera of the 2.5-m CMO telescope (Nadjip et al. 2017) using a 5-arcsec aperture (see Table 4). We present further photometry from 2022 to 2024 in Table 4 and Fig. 2: 29 epochs in the *J* band, 26 epochs in the *H* band, and 25 epochs in the *K* band. The observations were obtained with the same equipment and processed in the same way as previously.

**Table 5.** Results of the RM analysis with the MCCF code. The lags for the X data sets are measured with respect to the Y data and expressed in days. A positive lag means that variability of data set X follows that of data set Y. The peak correlation coefficient,  $R_{max}$ , is given along with the lags of the peak and centroid together with their confidence limits. Our preferred  $\tau_{peak}$  values are given in bold. All delays are reduced to the rest system. See the text for details.

X	Y	J.D.-2450000	Date	MCCF		
				$R_{max}$	$\tau_{peak}$	$\tau_{cent}$
I( <i>UVW1</i> )	I(X-ray)	9478–10381	2021 Sep–2024 Mar	0.856	<b>1.9</b> <sup>+1.3</sup> <sub>−0.4</sub>	0.6 <sup>+1.3</sup> <sub>−0.5</sub>
I( <i>B</i> )(CMO)	I(X-ray)	9495–10382	2021 Oct–2024 Mar	0.839	<b>2.2</b> <sup>+0.3</sup> <sub>−0.4</sub>	2.3 <sup>+0.2</sup> <sub>−0.2</sub>
I( <i>B</i> )(all)	I(X-ray)	9495–10382	2021 Oct–2024 Mar	0.780	<b>2.3</b> <sup>+0.2</sup> <sub>−0.2</sub>	2.0 <sup>+0.1</sup> <sub>−0.2</sub>
H $\beta$ (WIRO + CMO)	I(X-ray)	9517–10364	2021 Oct–2024 Mar	0.844	<b>7.3</b> <sup>+0.7</sup> <sub>−0.7</sub>	6.6 <sup>+0.3</sup> <sub>−0.3</sub>
H $\beta$ (WIRO + CMO)	I(X-ray)	9517–9698	2021 Oct–2022 Apr	0.889	<b>6.9</b> <sup>+1.6</sup> <sub>−0.4</sub>	6.3 <sup>+0.7</sup> <sub>−0.6</sub>
H $\beta$ (CMO)	I(X-ray)	10237–10364	2023 Oct–2024 Mar	0.945	<b>5.8</b> <sup>+0.9</sup> <sub>−1.4</sub>	5.8 <sup>+1.7</sup> <sub>−1.1</sub>
H $\beta$ /H $\alpha$ (CMO)	I(X-ray)	9517–1036	2021 Oct–2024 Mar	0.670	<b>7.0</b> <sup>+2.3</sup> <sub>−1.7</sub>	5.5 <sup>+1.3</sup> <sub>−0.2</sub>
I( <i>B</i> )(all)	I( <i>UVW1</i> )	9495–10382	2021 Oct–2024 Mar	0.834	<b>1.1</b> <sup>+0.3</sup> <sub>−0.1</sub>	1.1 <sup>+0.5</sup> <sub>−0.8</sub>
H $\beta$ (WIRO + CMO)	I( <i>UVW1</i> )	9517–10364	2021 Oct–2024 Mar	0.804	<b>4.6</b> <sup>+3.1</sup> <sub>−1.9</sub>	4.2 <sup>+2.1</sup> <sub>−2.3</sub>
H $\beta$ (WIRO + CMO)	I( <i>UVW1</i> )	9517–9698	2021 Oct–2022 Apr	0.855	<b>5.0</b> <sup>+2.0</sup> <sub>−2.0</sub>	4.3 <sup>+1.8</sup> <sub>−1.8</sub>
I( <i>J</i> ) (CMO)	I( <i>B</i> ) (CMO)	9514–10316	2021 Oct–2024 Jan	0.725	<b>5.4</b> <sup>+2.6</sup> <sub>−2.0</sub>	<b>5.2</b> <sup>+0.8</sup> <sub>−0.8</sub>
I( <i>H</i> ) (CMO)	I( <i>B</i> ) (CMO)	9514–10337	2021 Oct–2024 Jan	0.773	<b>15.1</b> <sup>+3.4</sup> <sub>−2.9</sub>	<b>15.3</b> <sup>+2.2</sup> <sub>−2.1</sub>
I( <i>K</i> ) (CMO)	I( <i>B</i> ) (CMO)	9514–10316	2021 Oct–2024 Jan	0.769	<b>14.2</b> <sup>+3.5</sup> <sub>−2.2</sub>	<b>15.5</b> <sup>+1.7</sup> <sub>−2.1</sub>
H $\beta$ (WIRO + CMO)	I( <i>B</i> ) (CMO)	9517–10364	2021 Oct–2024 Mar	0.758	<b>4.4</b> <sup>+2.6</sup> <sub>−0.4</sub>	3.3 <sup>+1.5</sup> <sub>−1.5</sub>
H $\beta$ (WIRO + CMO)	I( <i>B</i> ) (CMO)	9517–9698	2021 Oct–2022 Apr	0.882	<b>5.0</b> <sup>+1.3</sup> <sub>−1.7</sub>	4.6 <sup>+0.8</sup> <sub>−0.9</sub>
H $\beta$ (WIRO + CMO)	I( <i>B</i> ) (all)	9517–10364	2021 Oct–2024 Mar	0.769	<b>4.1</b> <sup>+1.6</sup> <sub>−0.6</sub>	3.6 <sup>+1.0</sup> <sub>−0.9</sub>

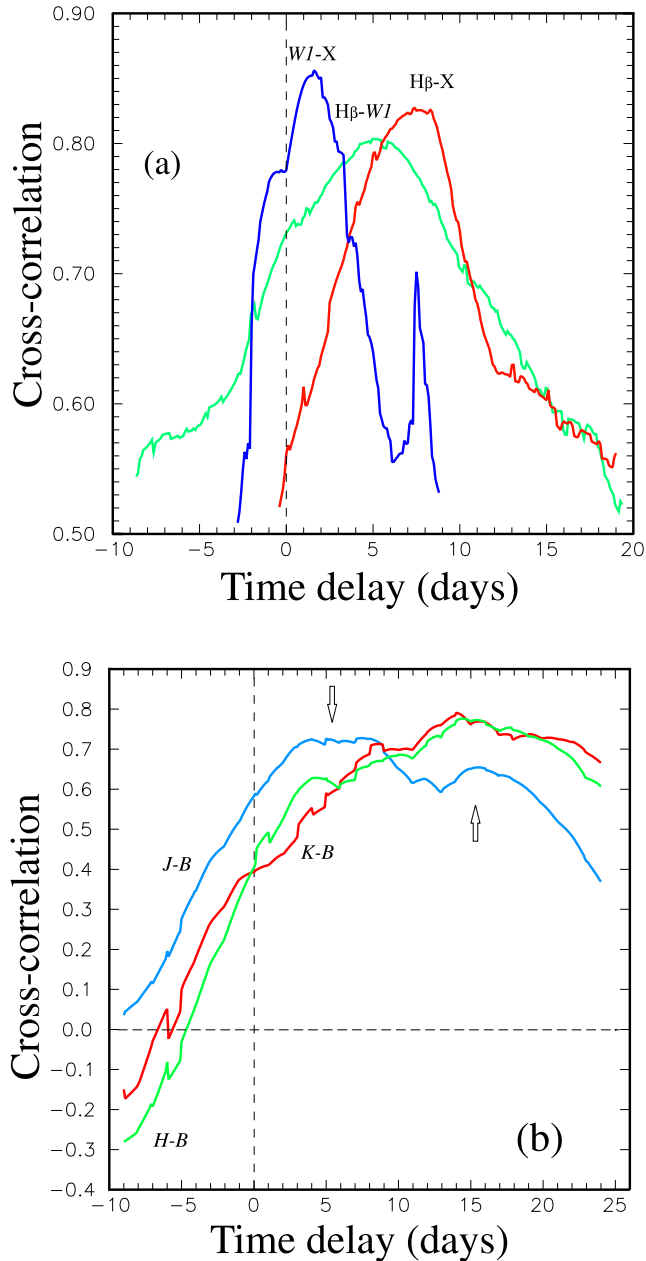


**Figure 3.** Some sample cross-correlation functions obtained with the MCCF method. Panel (a):  $(WI-X) - I(UVW1)$  from  $I(X\text{-ray})$ ,  $(H\beta-W1) - H\beta$  lagging  $I(UVW1)$ ,  $(H\beta-X) - H\beta$  lagging  $I(X\text{-ray})$ . Panel (b):  $(J-B) - I(J)$  lagging  $I(B)$ ,  $(H-B) - I(H)$  lagging  $I(B)$ ,  $(K-B) - I(K)$  lagging  $I(B)$ . All the data used for this plot are from CMO. For  $I(J)$ , one can see two peaks (at the delays of about 5.5 and 15 d), marked by arrows (see the Discussion section for details).

### 3 LIGHT CURVES AND TIME-SERIES ANALYSIS

#### 3.1 Light curves

The  $H\beta$  light curve for 2017–2024 is presented in Fig. 1 together with the  $UVW1$  intensity variation, and an enlargement of the 2021–2024 segment is shown in Fig. 1(b). The  $H\beta$  data obtained at different observatories are in a good agreement and correlate with UV variations on short and long time-scales. As it is well seen from the plots, the  $H\beta$  and UV variations demonstrate fast variability on

a time-scale of weeks, as well as a long-term trend of decreasing intensity on a time-scale of a few years.

The X-ray, UV, optical ( $B$  and  $\lambda 5200$  narrow band), IR ( $JHK$ ), and  $H\beta$  light curves during the last three seasons are given in Fig. 2. As can be seen from the optical light curve during 2021–2024, the  $B$  brightness was mostly low with low-amplitude (0.2–0.4 mag during 2021–2022 and then  $\sim 0.05$  mag during 2023–2024) fast and short variations on a time-scale of weeks. Over the same interval the X-ray flux varied significantly – by more than 20 times, and the amplitude of  $UVW1$  variations was larger than 1.5 mag. The variations at different wavelengths (from X-ray to near-IR) are well correlated at short (weeks) and long (a few years) time-scales. During the last season, the flux at all these wavelengths reached the lowest level ever observed over the entire period of monitoring. The X-ray flux at minimum was about two orders of magnitude lower than it was at maximum in 2013 (Shappee et al. 2014). The  $UVW1$  brightness dropped down by more than 3 magnitudes relative to the same maximum. The variability amplitude in the optical bands was lower (mostly due to a significant contamination from the host galaxy to the aperture photometry), but it was still more than one magnitude in the  $B$  band. One can well see a long-term significant decrease in 2021–2024 at all wavelengths on a time-scale of a few years in combination with fast brightenings on a time-scale of weeks. A significant fast X-ray brightening (by more than 30 times relative to minimal level) was detected in February 2024, which was followed by brightening at longer wavelengths and  $H\beta$ . Unfortunately, the maximal level in UV of the last fast brightening was missed due to the problems with the *Swift*/*UVOT* data. However, taking into account the high correlation of UV and X-ray variations, we estimate that the brightening in  $UVW1$  was about 1 mag.

#### 3.2 Reverberation-mapping method

To investigate lags between continuum variations at different wavelengths as traced by broad-band photometry from X-ray through UV and optical to near-IR, as well as between continuum and broad  $H\beta$ , we used the modernized cross-correlation function (MCCF) method (Oknyanskii 1993), which is an upgraded version of the traditional interpolation cross-correlation function (ICCF; Gaskell & Sparke 1986; Gaskell & Peterson 1987; Gaskell 1988) technique for two unevenly spaced data sets. The methodology of our analysis is mostly the same as described in our previous papers (see details and references, e.g. in Paper I). In this study, we use a publicly available PYTHON code implementing the MCCF (PyMCCF; see e.g. details in Paper II and Oknyansky & Oknyansky 2022). A small difference in the methodology compared to the previous paper is that we have de-trended all the light curves using a quadratic polynomial, which removes the substantial long-term decreasing trend (see Figs 1–2). We need to remove such trends because, if there is a strong trend in the series, the correlation coefficient is high over a wide lag interval. This leads to problems in our standard method of estimating errors for time delays since the errors are based on points with correlation coefficients larger than  $0.8R_{\max}$  (see e.g. Peterson et al. 1998).

#### 3.3 Time-delay measurements

The results of RM are presented in Table 5 and some of the results are plotted in Figs 3 and 4 (in combination with previously published results).

The X-ray flux led variations in the continuum at longer wavelengths and broad-line emission during 2021–2024: the  $UVW1$  variations lag by  $\sim 2.0$  d,  $B$  by  $\sim 2.3$  d, and  $H\beta$  by  $\sim 7.3$  d. These lags are in agreement with what was found in Paper II for 2017–2022.

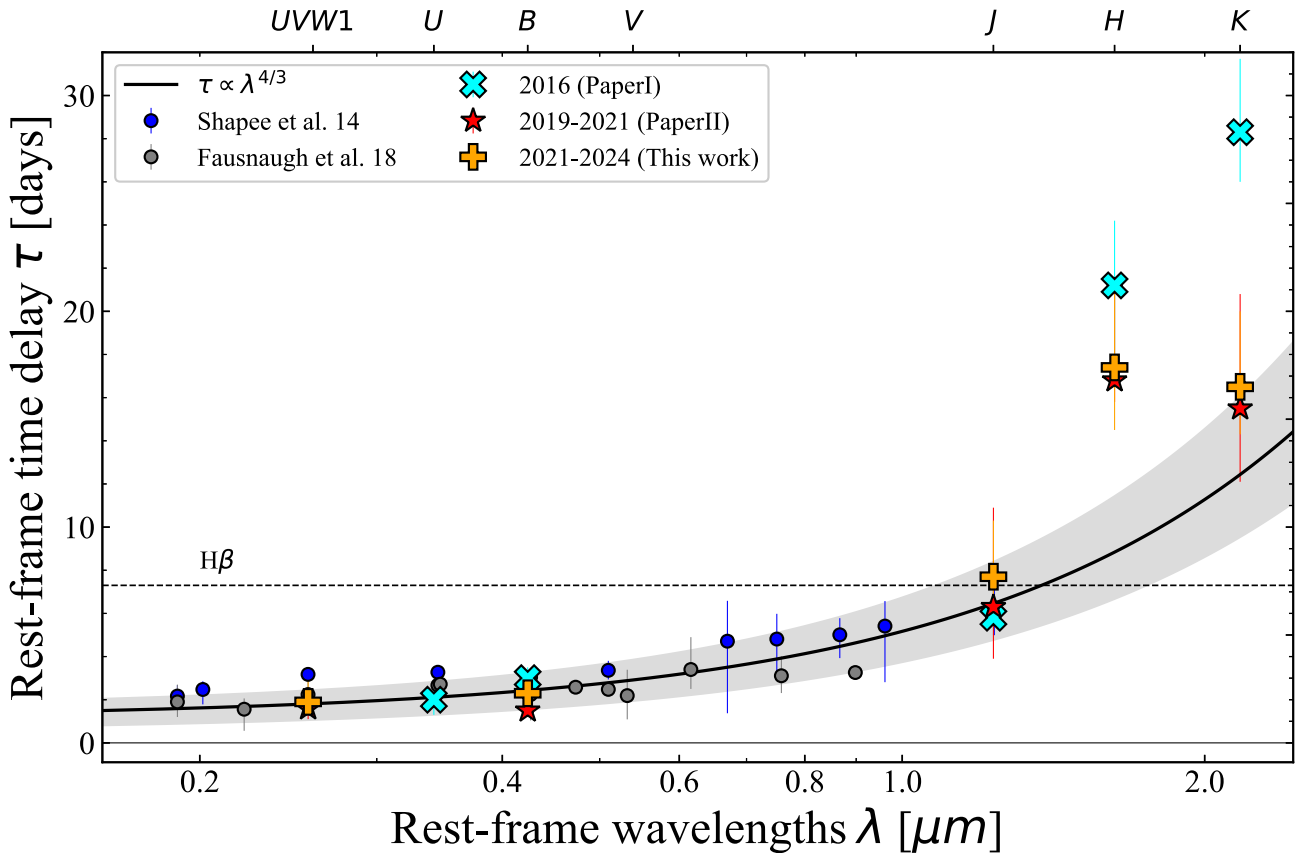


**Figure 4.** Lag-wavelengths relation relative to the X-ray flux based on the constraints reported in Table 5, and in previous publications. Open circles: Values from Fausnaugh et al. (2018). Filled circles: Values from Shappee et al. (2014) with omitting delays for  $H$  and  $K$  (see comments in Paper I). Time delays from our study: Paper I – crosses, Paper II – stars and this work – pluses. The horizontal dashed line marks the position of the average delay for  $H\beta$  obtained in Papers I and II. The best fit with the form  $\tau = a * \lambda^{4/3} + b$  combining all the available data (omitting  $JK$  delays) is shown as a bold line with the error marked as a grey area.

Also, the UV flux variability was followed in  $\sim 1.1$  d by the optical continuum variations ( $B$ ) and in  $\sim 4.6$  d by the  $H\beta$  variations. The optical variations ( $B$ ) were followed by the near-IR variability in  $\sim 5.5$  d in  $J$  and  $\sim 15$  d in  $HK$ , in  $\sim 4.4$  d by  $H\beta$ . The  $H\beta$  time delay is formally smaller than found in Paper II ( $\sim 6$  d) and by Li et al. (2024) ( $\sim 5.8$  d), but the difference is not very significant. Time-delay measurements were also carried out for a few shorter intervals (within individual seasons), but revealed no significant differences from the results for the three seasons combined. As it is shown in Fig. 4, the time delay for  $H\beta$  is bigger than for UV/Optical continuum but a few times smaller than for  $HK$ .

#### 4 EVOLUTION OF THE X-RAY/UV RELATION AND THE X-RAY SPECTRUM

In Paper II, we found a significant decrease of the  $F(UVW1)$  to  $F(X\text{-ray})$  ratio when NGC 2617 transitioned to the lower state. To trace the evolution of the UV/X-ray flux ratio, we plot the relation (see Fig. 5) for the last three seasons compared to the previous period 2017–2019 (see details in Paper II and Fig. 5). Evidently, the UV/X-ray ratio continued to decrease.

To trace the evolution of the X-ray spectrum of NGC 2617, we performed in Paper II a specific procedure. Here, we repeat the same analysis for the more recent seasons using specific *Swift*/XRT

observations at very low-flux levels (see Fig. 6). The amplitude of the photon-index variations is not large for NGC 2617 (see Paper II) compared to other CL AGNs (see e.g. Oknyansky et al. 2021 for NGC 3516). However, we noted some decrease of the photon index from  $\sim 1.85$  to  $\sim 1.30$  which followed the decrease in the X-ray flux from the high state to the deep minimum at the end of 2017 (see Paper II). We observed minima of the X-ray flux in 2023 that were several times lower than previously. For two of these epochs the exposures were sufficient to derive a photon-index value of  $1.85 \pm 0.15$ . At a confidence level of 95 per cent, this photon index is higher than 1.30, and at a confidence level of 99 per cent, we saw no difference from the photon index defined for the high state. That is in agreement with the expected ‘softer-when-fainter pattern’ at the very lowest count rates (Komossa et al. 2020).

#### 5 OPTICAL SPECTRAL VARIABILITY

##### 5.1 Broad emission-line profile variations and changing-look events

The large variation in the  $H\beta$  intensity (see Fig. 1 and fig. 2 in Paper II) was accompanied by significant changes in the line profile from 2017 to 2024 (see Figs 7–8 here and figs 8–9 in Paper II). Similar variations can be noted in broad  $H\gamma$  and a broad emission blend in

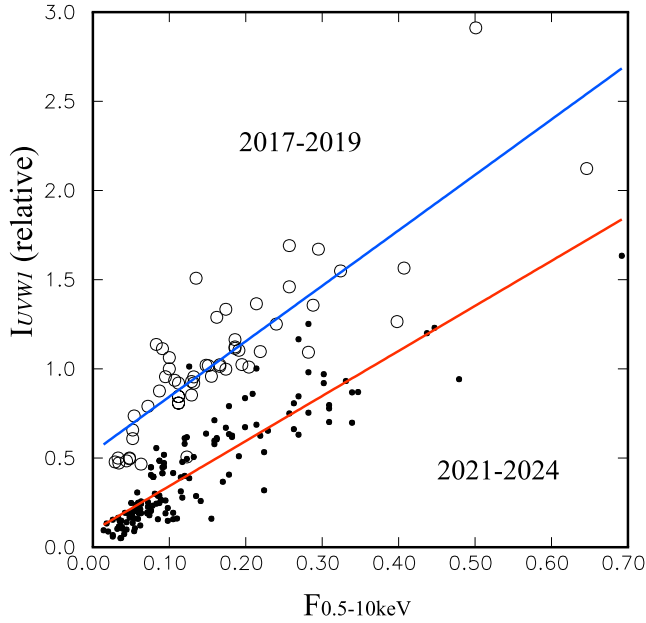


**Figure 5.** The relative intensity  $I(UVW1)$  versus (*Swift*) X-ray flux relation for two intervals: 2017 April–2019 November (open circles) and 2021 September–March 2024 (filled circles). The X-ray flux is given in units of  $10^{-10}$  erg  $s^{-1}$   $cm^{-2}$ . The  $I(UVW1)$  relative intensity is given in units  $I(15^m) = 1$  and is corrected for the host galaxy contamination. The straight lines (the blue line for the first interval and the red line for the second one) show regressions obtained by the least-squares method that minimize dispersion at  $I(UVW1)$ .

the region of He  $\lambda 5876$ . Broad H  $\alpha$  varied in the similar way but did not disappear at minimum (e.g. 06.01.2024) as did the broad H  $\beta$  (see Fig. 7).

H  $\beta$  profiles derived from the CMO spectra for the maximum, minimum, and the re-brightening states are presented in Fig. 8. We have removed narrow components as described in Paper II. As seen in the plot, the broad component of H  $\beta$  is barely detectable at minimum (2024 January 6 cf. 2021 October 29 when the object was at maximum), but became significant again after re-brightening (2024 February 20). These profiles illustrate two CL events: the first one – from type 1 (see Fig. 8b) (Shappee et al. 2014) to type 1.9, and then a rapid change to 1.5 on a time-scale of a month.

## 5.2 Variations of the H $\beta$ /H $\alpha$ ratio

The variation of the broad H  $\alpha$ /H  $\beta$  ratio based on the spectroscopic data obtained at WIRO and CMO in 2018–2022 was discussed in Paper II (fig. 13) where its anticorrelation with the UV flux was shown. Here in the Fig. 9, we prefer to show the variation of the broad H  $\beta$ /H  $\alpha$  ratio because of very low H  $\beta$  flux at minimum (see Fig. 1). We show this variation with the corresponding X-ray flux since some of the UV data were lost at particularly relevant brightening epochs due to problems with *Swift*/UVOT. The UV-flux variation is well correlated with the X-rays (see Fig. 3a), but with a short time-delay. So, even though we want to compare the H  $\beta$ /H  $\alpha$  ratio variation with the X-ray flux variation, this should correspond closely to a comparison with the UV flux variation. As one can see from Fig. 9, the H  $\beta$ /H  $\alpha$  ratio and X-ray flux show correlations. We find a delay of  $\sim 7$  d for this (see Table 5). This behaviour is in agreement with the anticorrelation between the H  $\alpha$ /H  $\beta$  ratio and the UV flux found in Paper II. There is an apparent correlation with both fast variations

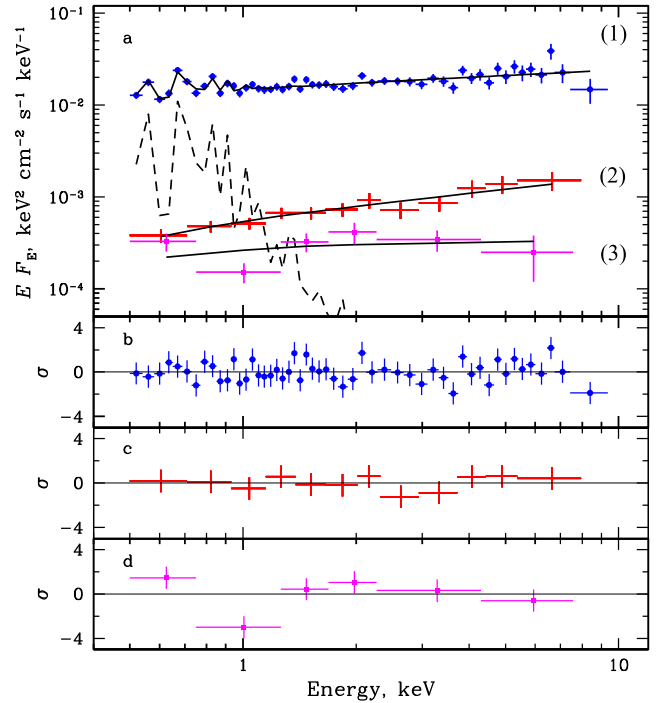


**Figure 6.** (a) Unfolded X-ray spectra of NGC 2617 obtained with *Swift*/XRT in the bright (ObsID 00032812008, 2013 May; (1) – blue points), mean-low (ObsID 00032812241–00032812246, December 2017; (2) – red points) and low (ObsID 00 010 549 158 and 00010549170, 2023 November–December; (3) – magenta points) states. The best-fitting models are shown with solid lines. The additional soft emission component in the bright state is shown with the dashed line. (b) Deviations of data from the absorbed power law with soft emission component in the bright state. (c) Deviations of data from the absorbed power law in the mean-low state. (d) Deviations of data from the simple absorbed power law in the low state. The (1), (2), (b), and (c) are the same as in fig. 15 of Paper II.

on a time-scale of weeks and longer variations on a time-scale of a few years.

## 6 DISCUSSION

The phenomenon of a single galaxy changing between types 1 and 2 characteristics at different time, as seen in NGC 2617, is indeed intriguing. NGC 2617 was observed to transition from a type 1.8 to a type 1 after an outburst in 2013, and then change back to a type 1.8/1.9 (with some strong variations) during the following decade, before returning quickly (on the time-scale of a few weeks) to a Sy 1.5 type after a strong and fast X-ray outburst in 2024 February. Such variability is not understood, but as discussed in the Introduction section, it challenges the simplest orientation unification model of thermal AGNs. Obviously, CL events cannot be explained by changing orientation which needs cosmological time, and so this phenomenon needs some other mechanism.

For NGC 2617 to undergo such a transformation, several scenarios have been proposed:

(1) Non-steady-state AD: A significant increase or decrease in the rate at which material is transferred through the disc and falls on to the supermassive black hole (SMBH) that alters the luminosity and the shape of the ionizing continuum, and thereby the appearance of the AGN.

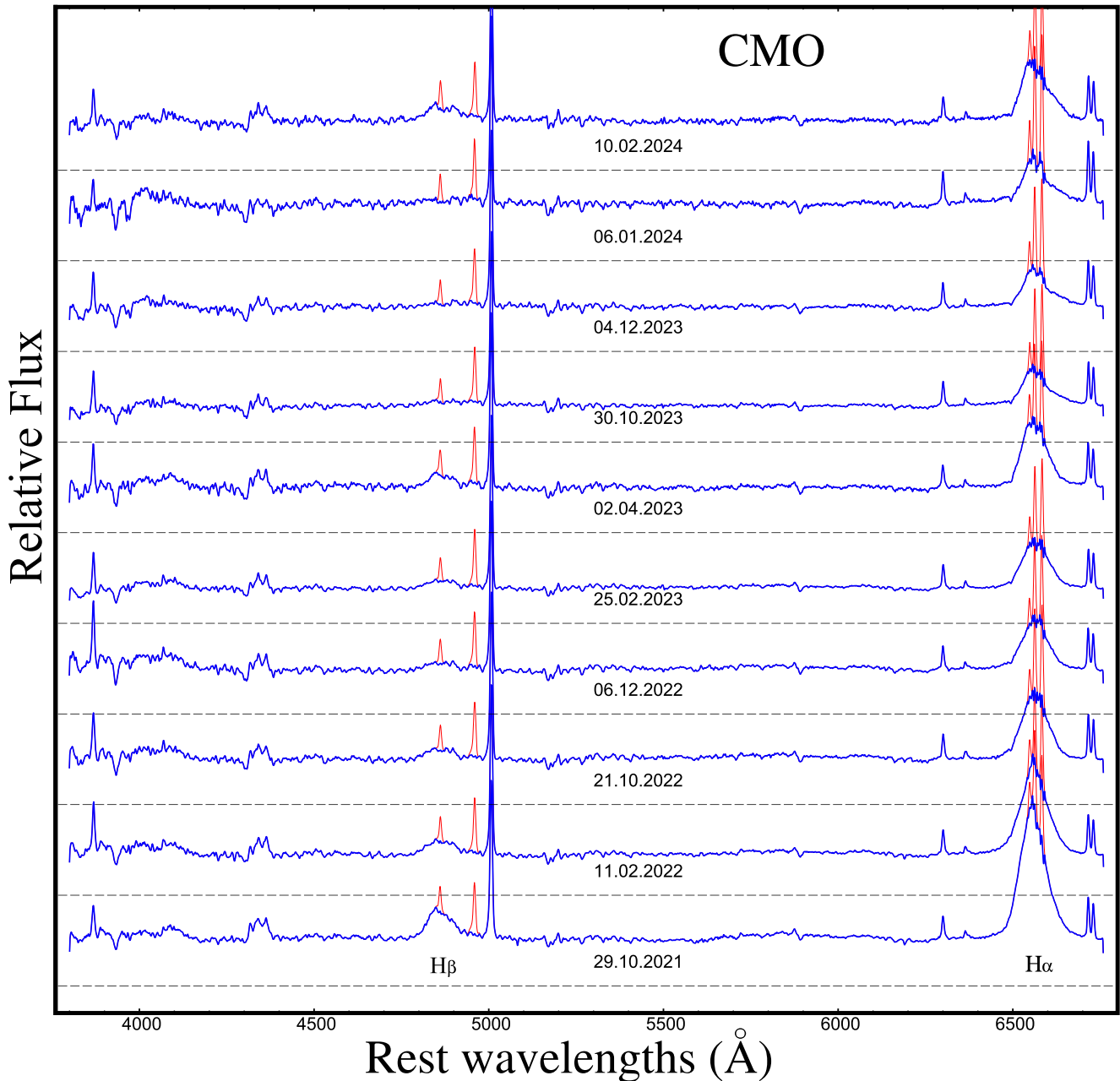


**Figure 7.** The  $H\beta$ – $H\alpha$  region of the selected spectra obtained at CMO. Spectra are normalized to the  $[O\text{ III}]\lambda 5007$  intensity and offset vertically for comparison. The bold lines show spectra with narrow lines blended with  $H\beta$  and  $H\alpha$  removed. The removed narrow components are shown by the thin lines. The dashed line below each spectrum indicates the zero flux level.

(2) Variable obscuration due to line-of-sight motions: Changes to the dust and gas columns that obscure the central region, which result from motions across the line of sight, revealing or hiding the BLR and AD.

(3) Variable obscuration induced by strong luminosity variations: Changes to the dust column along the sightlines resulting from dust recovery and/or sublimation, which is induced by fast and strong variations in luminosity, with the latter being the dominant driver for the CL event.

(4) Tidal disruption event (TDE): A star passing too close to the black hole could be torn apart, leading to a temporary change in the inflow rate of the accreted material, and to a change in the AGN’s properties.

(5) Stellar stripping: An event involving a more gentle (compared to a TDE) tidal stripping of stars (Ivanov & Chernyakova 2006; Campana et al. 2015), which can occur more frequently than TDE.

Taking into account that CL events happen recurrently in NGC 2617 as well as in several other CL AGNs (see e.g. Oknyansky 2022, and references therein), we can reject the TDE mechanism (4) as a plausible scenario for most CL events. Also, a TDE is inconsistent with the time-scales of the CL events observed in this object, and the strong long-term variations following the outburst in 2013 (as it is predicted the TDE event has to produce in the light curve a short plateau in maximum with a steep decline (see e.g. details Chan, Piran & Krolik 2020; Ricci & Trakhtenbrot 2023), which is not

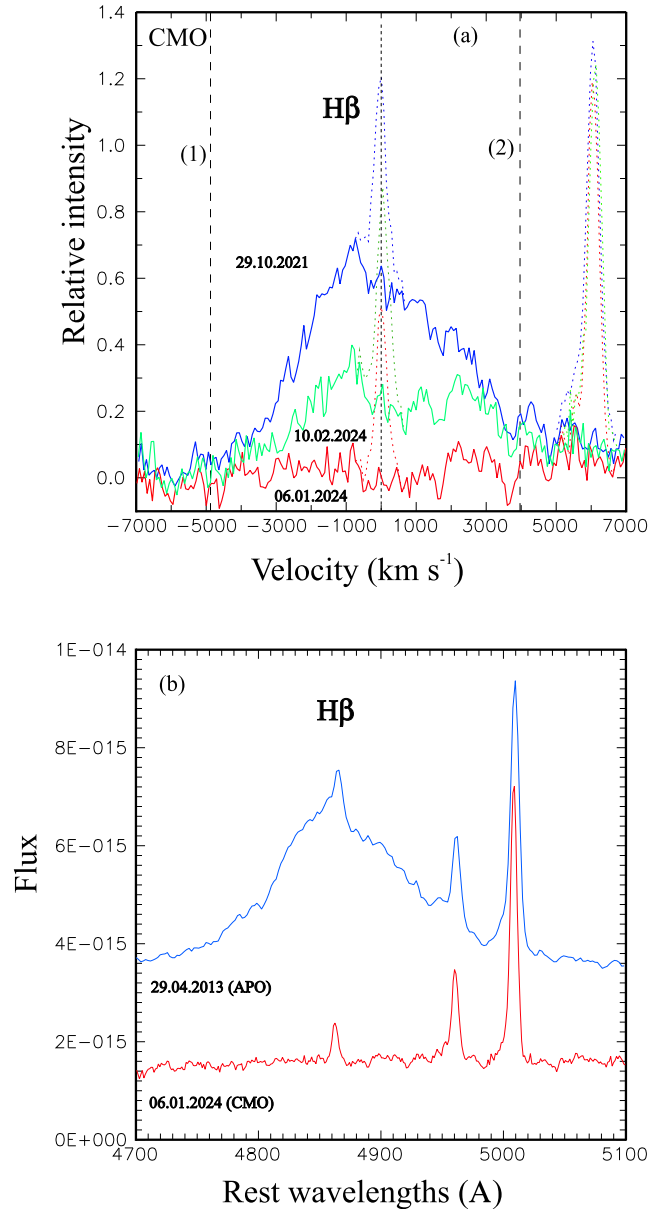


**Figure 8.** Panel (a) profiles, on a velocity scale, of broad H $\beta$  for the maximum (29.10.2021), minimum (06.01.2024), and post-minimum rebrightening states (10.02.2024) with the narrow components removed showing intrinsic variations of the line (data from CMO). The vertical dashed lines (1–2) mark the range of integration. See the text for details. Panel (b) profiles of H $\beta$  at minimum (CMO) and maximum (APO; Shappee et al. 2014). The flux is in units  $\text{erg s}^{-1} \text{cm}^{-2} \text{\AA}^{-1}$ .

the case for this object). For a TDE, strong helium emission lines must be present, but this is not the case for NGC 2617. Therefore, a more frequent mechanism than a tidally disrupted star is required to explain CL events, such as stellar stripping (5), which can also explain the recurrent nature of the phenomenon. Stellar stripping can also be a triggering mechanism for AD instabilities (1) leading to significant brightening of the source, and may also account for AGN fuelling. Stellar stripping can be one of the possible general mechanisms of AGN variability on a time-scale tens of years or more. Note that this scenario has not yet received sufficient theoretical research.

Understanding the high-amplitude variability of AGNs is crucial for our comprehension of the processes occurring in the vicinity of active SMBHs, as they drive the system away from equilibrium, potentially exposing non-linear effects and hinting at the natural scales of the system. Changes in the energy generation in AGNs are common, but the mechanism(s) driving the changes are not understood (see discussion and references on the topic of variability of CL AGNs in Gaskell & Klimek 2003; Gaskell 2008; Runnoe et al. 2016; Oknyansky et al. 2017b, 2019b, 2021; MacLeod et al. 2019; Ruan et al. 2019; Hon et al. 2022).

Variable obscuration due to dust clouds moving across our line of sight (2) cannot be a *dominant* cause for the variability of NGC 2617 due to the discrepancy between the time-scales predicted by the model  $\sim 7$  yr (see e.g. details in Feng et al. 2021) and the observed ones (changing from type 1.8 to type 1.9 during about 1 yr and then to type 1.5 during about a few weeks). Also, clear evidence that X-ray variations drive continuum and emission-line variability at longer wavelengths cannot be explained by variable obscuration. For a more detailed discussion of the possible mechanisms underlying the CL phenomenon and for additional references, see Paper II.

The CL Seyfert galaxy NGC 2617 has been the subject of extensive study over the last decade (after the realization of its CL nature by Shappee et al. 2014) due to its large-amplitude variability. The X-ray and UV/optical variability of NGC 2617 is not unusual for a CL AGN. There are dramatic changes in the X-ray flux, varying by about two orders of magnitude. These changes are correlated with variations at UV, optical wavelengths and broad emission lines with some delays.

The relationship between X-ray flux of thermal AGNs and the flux at lower energies (in the UV and optical) is complicated. As Gaskell (2006) summarized, short-term variations of the X-ray and optical fluxes *can* be correlated but they can also be *uncorrelated*. Periods of correlation and lack of correlation (or even anticorrelation) can be found in the some AGNs.

Not surprisingly, the UV/X-ray ratio can dramatically change in some CL AGNs during the type transition processes. Variable obscuration due to recovering of the dust in low state may explain the decrease of the UV/X-ray flux ratio found in our study and some previous work: NGC 2617 (Paper II) and NGC 1566 (Oknyansky et al. 2020b).

Short time lags indicate that rapid variability across different wavebands (from X-rays to UV/optical) in AGNs is primarily driven by variable illumination of the AD by soft X-rays, although the *detailed* variability often does not match up (see fig. 3 in Gaskell 2006). In summary, NGC 2617’s behaviour aligns with the typical characteristics of thermal AGNs in general and CL AGNs in particular, and its variability is influenced by the interaction between X-rays and the accretion disc (see Fig. 4). Our RM results are in agreement with the disc reprocessing model, which predicts an increase in lag with wavelength and a high correlation between X-ray and UV/optical variability. We have found a time delay between X-ray and UV variations of about 2 d (which is in agreement with previously published results; Shappee et al. 2014; Kammoun, Papadakis & Dovčiak 2021) and a relatively short lag of  $\sim 1$  d (or less, see Paper II) delay between UV and optical band variability. This result (combination of too long X-ray to UV delay with short UV/optical lag) is in contradiction with the simplest, commonly-invoked ‘lamp post’ model (see e.g. details in Cackett, Horne & Winkler 2007). This problem is well known (see e.g. our discussion in Paper II and Shappee et al. 2013a; McHardy et al. 2014; Shappee et al. 2014; Buisson et al. 2017; Edelson et al. 2017; Oknyansky et al. 2017b, 2020b, 2021;

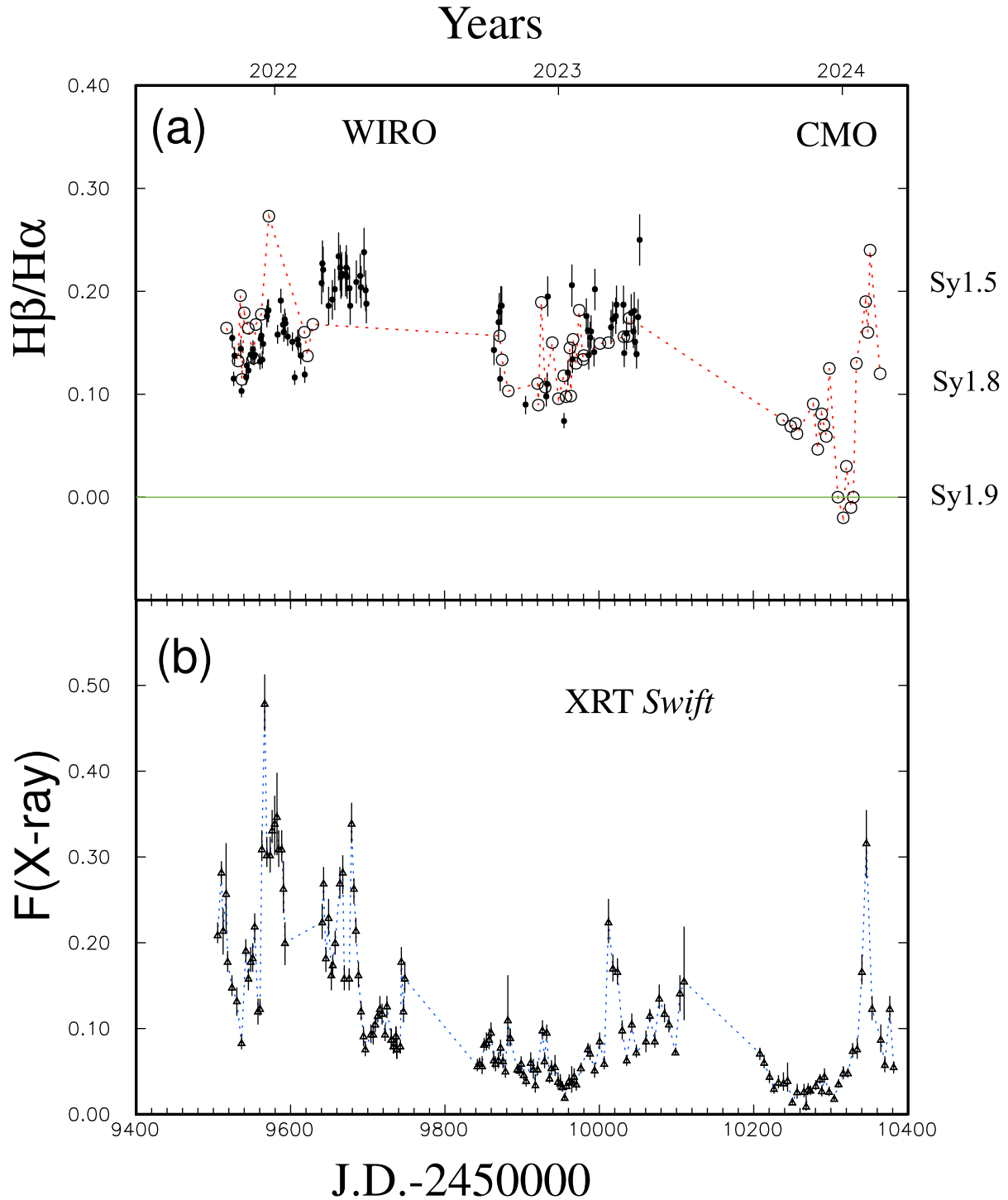


**Figure 9.** Panel (a): Variation of the  $H\beta/H\alpha$  ratio (broad) during 2021–2024 (points–WIRO, open circles–CMO). The WIRO data were reduced to the CMO system for broad  $H\beta$  and  $H\alpha$ . The horizontal reference (narrow) line shows the level  $H\beta/H\alpha = 0$ . Panel (b): Variation of the (*Swift*) X-ray flux (triangles) in the range of 0.5–10 keV during 2021–2024 in units of  $10^{-10} \text{ erg s}^{-1} \text{ cm}^{-2}$ .

Lawther et al. 2022; Oknyansky 2022). Furthermore, the  $\sim 2$  d delays between X-ray and UV/optical bands are significantly larger, by nearly an order of magnitude, compared to the predictions of a standard irradiated thin AD (Fian et al. 2022, and references therein), if the observed optical luminosity of the source of  $\sim 8 \times 10^{42} \text{ erg s}^{-1}$  is a representative nuclear luminosity (Shappee

et al. 2013b). Similar, albeit somewhat smaller discrepancies have been noted also for non-CL AGNs (Gaskell 2017; Chelouche, Pozo Nuñez & Kaspi 2019; Fian, Chelouche & Kaspi 2023, and references therein).

One of the possible solutions (Gaskell 2017) to this ‘accretion-disc-size problem’ is simply that the luminosity of AGNs has

been substantially underestimated by ignoring significant internal extinction (see especially Gaskell et al. 2023). Alternatively, this problem can be probably solved in the revised lamp post model (see e.g. Starkey et al. 2023). There are at least three other possible mechanisms that have been discussed in literature: (1) an X-ray source at a large height (about 2 light-days) from the SMBH, (2) a truncated (at the inner edge) AD in analogy with black-hole binaries (e.g. Done, Gierliński & Kubota 2007), and (3) a model with a soft-excess emitting region at the inner edge of an AD which completely hides the hard X-ray corona (Edelson et al. 2017; Gardner & Done 2017). These options were considered by Noda et al. (2016) who preferred explanation (2). In Paper II, we find model (3) to be consistent with our data for NGC 2617 (as well as for NGC 3516) implying soft variable black-body components in the X-ray spectra, which agree with the model’s predictions (see details in Paper II and Oknyansky 2022).

An additional option to resolving the accretion-disc-size conundrum is the contamination of the UV and optical bands by a delayed varying flux component originating from diffuse continuum emission from the BLR leading to longer delays (Korista & Goad 2001; Cackett et al. 2018; Lawther et al. 2018; Chelouche et al. 2019; Netzer 2022). It is unclear how important this mechanism is for NGC 2617 in its low state given that its small UV bump is not conspicuous in individual spectra (and the root mean square spectrum is of poor quality). Similarly, it is unclear whether this process can explain the UV-to-optical delays (in the low state, however may work in the high state as suggested by Netzer 2022).

The near-IR variability of NGC 2617 is also typical for AGNs. Time delays in near IR ( $HK$ ) are relatively wavelength independent (see e.g. Oknyansky et al. 2019a) and a few times longer than the delays in broad Balmer emission lines. For the shortest near-IR wavelengths ( $J$ ) we found two different time delays (Fig. 3b): a long one of about 15 d is about the same as for  $HK$  (which is suspected to be connected with thermal re-radiation by the dust), and the shortest delay is about 6 d (probably connected with radiation from the edge of the AD). This delay is in agreement with that found by Shappee et al. (2014) who considered it as an estimate of the AD size. As for the UV-to-optical time-delays, the implied AD size is a factor of  $\sim 8$  larger than predicted by standard AD models. The AD size can be a few times bigger than is expected in the standard model due to X-ray illumination (see e.g. Papadakis, Dovčiak & Kammoun 2022), but it is unlikely to explain the large factor implied for NGC 2617. The value of the dust time delay changes with the UV luminosity with some delay (see e.g. Oknyansky & Gaskell 2024, and references therein). These properties are also common for AGNs (e.g. NGC 4151, NGC 3516).

The apparent strong variability of the Balmer lines in NGC 2617 is similar to that reported previously for some other CL AGNs. In most of the observed CL events the broad  $H\alpha$  line is prominent in the minima when the broad  $H\beta$  line is marginal or absent. At minima, some CL AGNs change their type to type 1.8–type 1.9 with a very small  $H\beta/H\alpha$  ratio what is typical for such objects. Apparently strong variability in the Balmer decrement as in NGC 2617 is a typical property of CL AGNs (see recent publication on the subject by Li et al. (2024), discussion and references in Paper II). This phenomenon can be explained by at least two different mechanisms: (1) variable dust extinction (Goodrich 1995; Kollatschny, Bischoff & Dietrich 2000) and (2) ionizing effect (see e.g. Shapovalova et al. 2010; Ilić et al. 2012). These two mechanisms can work in tandem as well. Fast variation on a time-scale of a few

months are rather connected with the second option, but variation on a time-scale of a few years can be connected with variable dust obscuration.

## 7 SUMMARY

Using spectroscopy and multiwavelength photometry, we have shown that NGC 2617 continued to be mostly in a relatively low-flux state in 2021–2024 with the broad  $H\beta$  line being very weak. We observed two CL events for the object during this interval: changing from type 1.8 (Paper II) to type 1.9 in 2024 January and then changing back to type 1.5 in 2024 February. The duration of the high state and the continuing variability are not readily consistent with the suggestion that the type change is due to a TDE.

We proposed in Papers I and II that (1) the initial change of object type (Shappee et al. 2014) was the result of increased luminosity which caused the sublimation of dust in the inner part of a biconical dusty outflow. This makes its central regions much more visible. (2) The object has to be in a low state at least for a few years so that the dust can recover and obscure the broad lines more significantly. The combination of low luminosity (as a dominant reason) with more significant dust obscuration leads to a CL event, which is what we observed as had been predicted and expected before.

We have found at the interval 2021–2024 that near-IR time delay became significantly shorter (15 d) than it was in 2016 (24 d), which is also in agreement with possible dust recovery. In the case of variable absorption, the UV/X-ray ratio also has to drop down, as it has been found here and in Paper II.

## ACKNOWLEDGEMENTS

We thank A. Cherepashchuk for supporting our research and observations, and the staff of the observatories. We also express our thanks to the *Swift* administrators for approving the ToO observation requests and the *Swift* ToO team for promptly scheduling and executing our observations. We thank B. Shappee for sending us data in a digital format. We are grateful to H. Netzer and A. Laor for useful discussions. This work was supported in part by the M. V. Lomonosov Moscow State University Program of Development. This research has been partly supported by Israeli Science Foundation grants 2398/19, 1650/23, and by the Center for Integration in Science of the Ministry of Aliyah and Integration. We thank WIRO engineers Conrad Vogel and Andrew Hudson for their indispensable and invaluable assistance. M.S. Brotherton enjoyed support from the Chinese Academy of Sciences Presidents International Fellowship Initiative (grant 2018VMA0005). T.E. Zastrocky acknowledges support from NSF grant 1005444I. We thank H. Winkler and F. van Wyk as the data providers and the South African Astronomical Observatory (SAAO) for the allocation of telescope time and use of their facilities. P. Du acknowledges financial support from National Key R&D Program of China (2023YFA1607903 and 2021YFA1600404), from NSFC grants NSFC-12022301 and 11991051, and by the China Manned Space Project with no. CMS-CSST-2021-A06. J.-M. Wang acknowledges financial support from National Key R&D Program of China 2021YFA1600404, from NSFC grants NSFC 11991050, 11991054 and 12333003, and by the China Manned Space Project with no. CMS-CSST-2021-A06.

## DATA AVAILABILITY

The data underlying this study are available in the main body of the article and in online supplementary material.

## REFERENCES

- Andrillat Y., Souffrin S., 1968, *ApJ*, 1, 111
- Antonucci R., 1993, *ARA&A*, 31, 473
- Antonucci R., 2012, *Astron. Astrophys. Trans.*, 27, 557
- Brosch N., Kaspi S., Niv S., Manulis I., 2015, *Ap&SS*, 359, 9
- Buisson D. J. K., Lohfink A. M., Alston W. N., Fabian A. C., 2017, *MNRAS*, 464, 3194
- Cackett E. M., Horne K., Winkler H., 2007, *MNRAS*, 380, 669
- Cackett E. M., Chiang C.-Y., McHardy I., Edelson R., Goad M. R., Horne K., Korista K. T., 2018, *ApJ*, 857, 53
- Campana S., Mainetti D., Colpi M., Lodato G., D’Avanzo P., Evans P. A., Moretti A., 2015, *A&A*, 581, A17
- Chan C.-H., Piran T., Krolik J. H., 2020, *ApJ*, 903, 17
- Chelouche D., Pozo Nuñez F., Kaspi S., 2019, *Nat. Astron.*, 3, 251
- Chuvaev K. K., 1991, *Bull. Crimean Astrophys. Obs.*, 83, 177
- Chuvaev K. K., Oknyanskii V. L., 1989, *Soviet Ast.*, 33, 1
- Denney K. D. et al., 2014, *ApJ*, 796, 134
- Done C., Gierliński M., Kubota A., 2007, *A&AR*, 15, 1
- Du P. et al., 2018, *ApJ*, 869, 142
- Edelson R. et al., 2017, *ApJ*, 840, 41
- Fausnaugh M. M., 2017, PhD thesis, The Ohio State University
- Fausnaugh M. M. et al., 2018, *ApJ*, 854, 107
- Feng H.-C. et al., 2021, *ApJ*, 912, 92
- Fian C., Chelouche D., Kaspi S., Sobrino Figaredo C., Catalan S., Lewis T., 2022, *A&A*, 659, A13
- Fian C., Chelouche D., Kaspi S., 2023, *A&A*, 677, A94
- Gardner E., Done C., 2017, *MNRAS*, 470, 3591
- Gaskell C. M., 1988, *ApJ*, 325, 114
- Gaskell C. M., 2006, in Gaskell C. M., McHardy I. M., Peterson B. M., Sergeev S. G., eds, *ASP Conf. Ser. Vol. 360, AGN Variability from X-Rays to Radio Waves*. Astron. Soc. Pac., San Francisco, p. 111
- Gaskell C. M., 2008, *Rev. Mex. Astron. Astrofis.*, 32, 1, preprint (arXiv:0711.2113)
- Gaskell C. M., 2017, *MNRAS*, 467, 226
- Gaskell C. M., Klimek E. S., 2003, *Astron. Astrophys. Trans.*, 22, 661
- Gaskell C. M., Peterson B. M., 1987, *ApJS*, 65, 1
- Gaskell C. M., Sparke L. S., 1986, *ApJ*, 305, 175
- Gaskell C. M., Anderson F. C., Birmingham S. Á., Ghosh S., 2023, *MNRAS*, 519, 4082
- Giustini M. et al., 2017, *A&A*, 597, A66
- Goodrich R. W., 1995, *ApJ*, 440, 141
- Hon W. J., Wolf C., Onken C. A., Webster R., Auchettl K., 2022, *MNRAS*, 511, 54
- Ilić D., Popović L. Č., La Mura G., Ciroi S., Rafanelli P., 2012, *A&A*, 543, A142
- Ivanov P. B., Chernyakova M. A., 2006, *A&A*, 448, 843
- Kammoun E. S., Papadakis I. E., Dovčiak M., 2021, *MNRAS*, 503, 4163
- Keel W. C., 1980, *AJ*, 85, 198
- Khachikian E. Y., Weedman D. W., 1971, *ApJ*, 164, L109
- Khachikyan É. Y., Weedman D. W., 1971, *Astrophysics*, 7, 231
- Klimek E. S., Gaskell C. M., Hedrick C. H., 2004, *ApJ*, 609, 69
- Kokubo M., Minezaki T., 2020, *MNRAS*, 491, 4615
- Kollatschny W., Bischoff K., Dietrich M., 2000, *A&A*, 361, 901
- Komossa S. et al., 2020, *A&A*, 643, L7
- Korista K. T., Goad M. R., 2001, *ApJ*, 553, 695
- LaMassa S. M. et al., 2015, *ApJ*, 800, 144
- Lawther D., Goad M. R., Korista K. T., Ulrich O., Vestergaard M., 2018, *MNRAS*, 481, 533
- Lawther D., Vestergaard M., Raimundo S., Koay J. Y., Peterson B. M., Fan X., Grupe D., Mathur S., 2023, *MNRAS*, 519, 3903
- Li S.-S. et al., 2024, *ApJ*, 972, 105
- López-Navas E. et al., 2023, *MNRAS*, 524, 188
- Ljutij V. M., Oknyanskij V. L., Chuvaev K. K., 1984, *Sov. Astron. Lett.*, 10, 335
- MacLeod C. L. et al., 2016, *MNRAS*, 457, 389
- MacLeod C. L. et al., 2019, *ApJ*, 874, 8
- Mathur S. et al., 2013, *Astron. Telegram*, 5039, 1
- McHardy I. M. et al., 2014, *MNRAS*, 444, 1469
- Moran E. C., Halpern J. P., Helfand D. J., 1996, *ApJS*, 106, 341
- Nadjip A. E., Tatarnikov A. M., Toomey D. W., Shatsky N. I., Cherepashchuk A. M., Lamzin S. A., Belinski A. A., 2017, *Astrophys. Bull.*, 72, 349
- Netzer H., 2022, *MNRAS*, 509, 2637
- Noda H. et al., 2016, *ApJ*, 828, 78
- Oknyanskii V. L., 1993, *Astron. Lett.*, 19, 416
- Oknyanskij V. L. et al., 2016, *Odessa Astron. Publ.*, 29, 92
- Oknyansky V., 2022, *Astron. Nachr.*, 343, e210080
- Oknyansky V. L., Gaskell C. M., 2024, in Bruni G., Diaz Trigo M., Laha S., Fukumura K., eds, *IAU Symposium Vol. 378, IAU Symposium*, Cambridge Univ. Press, Cambridge, p. 3
- Oknyansky V., Oknyansky R., 2022, *Astrophysics Source Code Library*, recordascl:2212.007
- Oknyansky V. L., Gaskell C. M., Shimanovskaya E. V., 2015, *Odessa Astron. Publ.*, 28, 175
- Oknyansky V. L. et al., 2017a, *Odessa Astron. Publ.*, 30, 117(Paper I)
- Oknyansky V. L. et al., 2017b, *MNRAS*, 467, 1496
- Oknyansky V. L., Malanchev K. L., Gaskell C. M., 2018, *PoS*, NLS1-2018, 12
- Oknyansky V. L., Shenavrin V. I., Metlova N. V., Gaskell C. M., 2019a, *Astron. Lett.*, 45, 197
- Oknyansky V. L., Winkler H., Tsygankov S. S., Lipunov V. M., Gorboskovy E. S., van Wyk F., Buckley D. A. H., Tyurina N. V., 2019b, *MNRAS*, 483, 558
- Oknyansky V. L., Mikailov K. M., Huseynov N. A., 2020a, *Astron. Rep.*, 64, 979
- Oknyansky V. L. et al., 2020b, *MNRAS*, 498, 718
- Oknyansky V. L. et al., 2021, *MNRAS*, 505, 1029
- Oknyansky V. L. et al., 2023a, *MNRAS*, 525, 2571(Paper II)
- Oknyansky V. L. et al., 2023b, *Astron. Telegram*, 16324, 1
- Olson K. et al., 2020, in *American Astronomical Society Meeting Abstracts #235*, p. 304.01
- Osterbrock D. E., 1981, *ApJ*, 249, 462
- Osterbrock D. E., 1987, in Khachikian E. E., Fricke K. J., Melnick J., eds, *IAU Symp. Vol. 121, Observational Evidence of Activity in Galaxies*. Cambridge Univ. Press, Cambridge, p. 109
- Papadakis I. E., Dovčiak M., Kammoun E. S., 2022, *A&A*, 666, A11
- Pastoriza M., Gerola H., 1970, *ApJ*, 6, 155
- Paturel G., Theureau G., Bottinelli L., Gougouenheim L., Coudreau-Durand N., Hallet N., Petit C., 2003, *A&A*, 412, 57
- Penston M. V., Perez E., 1984, *MNRAS*, 211, 33P
- Peterson B. M., Wanders I., Horne K., Collier S., Alexander T., Kaspi S., Maoz D., 1998, *PASP*, 110, 660
- Pozo Nuñez F., Chelouche D., Kaspi S., Niv S., 2017, *PASP*, 129, 094101
- Pronik V. I., Chuvaev K. K., 1972, *Astrophysics*, 8, 112
- Raimundo S. I., Vestergaard M., Koay J. Y., Lawther D., Casasola V., Peterson B. M., 2019, *MNRAS*, 486, 123
- Ricci C., Trakhtenbrot B., 2023, *Nat. Astron.*, 7, 1282
- Ruan J. J., Anderson S. F., Eracleous M., Green P. J., Haggard D., MacLeod C. L., Runnoe J. C., Sobolewska M. A., 2019, *ApJ*, 883, 76
- Runnoe J. C. et al., 2016, *MNRAS*, 455, 1691
- Shapovalova A. I., Popović L. Č., Burenkov A. N., Chavushyan V. H., Ilić D., Kovačević A., Bochkarev N. G., León-Tavares J., 2010, *A&A*, 509, A106
- Shapovalova A. I. et al., 2019, *MNRAS*, 485, 4790
- Shappee B. J. et al., 2013a, *Astron. Telegram*, 5010
- Shappee B. J. et al., 2013b, *Astron. Telegram*, 5059, 1
- Shappee B. J. et al., 2014, *ApJ*, 788, 48
- Sheng Z., Wang T., Jiang N., Yang C., Yan L., Dou L., Peng B., 2017, *ApJ*, 846, L7
- Starkey D. A., Huang J., Horne K., Lin D. N. C., 2023, *MNRAS*, 519, 2754
- Tsygankov S., Krivonos R., Sazonov S., Lutovinov A., Sunyaev R., 2013, *Astron. Telegram*, 5103, 1
- Veronese S., Vignali C., Severgnini P., Matzeu G. A., Cignoni M., 2024, *A&A*, 683, A131
- Wang J.-M., Bon E., 2020, *A&A*, 643, L9

Yang J., Paragi Z., Komossa S., van Bemmel I., Oonk R., 2013, *Astron. Telegram*, 5125, 1  
Yang J. et al., 2021, *MNRAS*, 503, 3886

## SUPPORTING INFORMATION

Supplementary data are available at [MNRAS](#) online.

## suppl\_data

Please note: Oxford University Press is not responsible for the content or functionality of any supporting materials supplied by the authors. Any queries (other than missing material) should be directed to the corresponding author for the article.

This paper has been typeset from a  $\text{\TeX}/\text{\LaTeX}$  file prepared by the author.